Available on CMS information server

CMS NOTE 2007/031

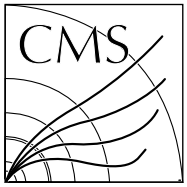

The Compact Muon Solenoid Experiment

CMS Note

Mailing address: CMS CERN, CH-1211 GENEVA 23, Switzerland

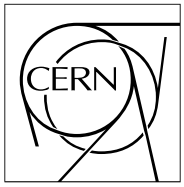

17 October 2007

Efficiency of Finding Muon Track Trigger Primitives in CMS Cathode Strip Chambers

R. Breedon, P. T. Cox, B. Holbrook, W. Ko, M. Tripathi

University of California, Davis, California 95616, USA

V. Andreev, D. Cline, R. Cousins, J. Hauser, M. Ignatenko, G. Rakness, J. Tucker, V. Valuev, M. von der Mey, Y. Zheng

University of California, Los Angeles, California 90024, USA

R. Clare, D. Fortin, S.-C. Kao, V. Sytnik

University of California, Riverside, California 92521, USA

T. Ferguson, N. Terentyev, I. Vorobiev

Carnegie Mellon University, Pittsburgh, Pennsylvania 15213, USA

G. Apollinari, I. Bloch, D. Eartly, F. Geurts, S. Lusin, Yu. Pischalnikov, O. Prokofiev

Fermi National Accelerator Laboratory, Batavia, Illinois 60510, USA

D. Acosta, V. Barashko, P. Bartalini, A. Drozdetskiy, D. Holmes, K. Kotov, A. Korytov, P. Levchenko, A. Madorsky, G. Mitselmakher, Yu. Pakhotin[1)], D. Wang

University of Florida, Gainesville, Florida 32611, USA

M. Chen, K. He, C. Jiang, H. Sun, W. Zhao, Z. Zhu

Institute of High Energy Physics, Beijing, People's Republic of China

Yu. Ershov, I. Golutvin, V. Karjavin, S. Khabarov, P. Moisenz, V. Perelygin, V. Tchekhovski, S. Vassiliev, A. Zarubin

Joint Institute for Nuclear Research, Dubna, Russia

E. Barberis, O. Boeriu, A. Roe

Northeastern University, Boston, Massachusetts 02115, USA

M. Schmitt, S. Stoynev

Northwestern University, Evanston, Illinois 60208, USA

[1)] Contact person. e-mail: pakhotin@ufl.edu

B. Bylsma, S. Durkin, J. Gilmore, J. Gu, P. Killewald, T.Y. Ling, G.L. Williams

The Ohio State University, Columbus, Ohio 43210, USA

N. Bondar, A. Denisov, V. Golovtsov, Yu. Ivanov, A. Petrunin, A. Schetkovsky, L. Schipunov, V. Sknar, V. Sulimov, L. Uvarov, S. Vavilov, G. Velichko, S. Volkov, A. Vorobyev, An. Vorobyev, V. Yatsura, G. Zhmakin

Petersburg Nuclear Physics Institute, St. Petersburg, Russia

A. Adam, K. Banicz, A. Bujak, L. Gutay, N. Ippolito, Yu. Kozhevnikov, S. Medved, I. Pal, G. Zilizi

Purdue University, West Lafayette, Indiana 47907, USA

J. Liu, M. Matveev, B. P. Padley, J. Roberts, A. Tumanov

Rice University, Houston, Texas 77005, USA

A. Golyash, J. Pivarsky, A. Safonov

Texas A&M University, College Station, Texas 77843, USA

Y. Baek, A. Lanaro, R. Loveless

University of Wisconsin, Madison, Wisconsin 53706, USA

Abstract

In the CMS Experiment, muon detection in the forward direction is accomplished by cathode strip chambers (CSC). These detectors identify muons, provide a fast muon trigger, and give a precise measurement of the muon trajectory. There are 468 six-plane CSCs in the system. The efficiency of finding muon trigger primitives (muon track segments) was studied using 36 CMS CSCs and cosmic ray muons during the Magnet Test and Cosmic Challenge (MTCC) exercise conducted by the CMS experiment in 2006. In contrast to earlier studies that used muon beams to illuminate a very small chamber area (< 0.01 m^2), results presented in this paper were obtained by many installed CSCs operating *in situ* over an area of ≈ 23 m^2 as a part of the CMS experiment. The efficiency of finding 2-dimensional trigger primitives within 6-layer chambers was found to be $99.93 \pm 0.03\%$. These segments, found by the CSC electronics within 800 ns after the passing of a muon through the chambers, are the input information for the Level-1 muon trigger and, also, are a necessary condition for chambers to be read out by the Data Acquisition System.

To be submitted to *NIM*

1 Introduction

The Endcap Muon (EMU) system [1, 2, 3] of the Compact Muon Solenoid (CMS) experiment [4] is now being commissioned for the Large Hadron Collider (LHC) [5]. The technology chosen for the EMU system is cathode strip chambers (CSC) [6, 7], the concept of which was first proposed by G. Charpak more than 30 years ago [8]. The CMS CSCs will detect muons in the pseudorapidity [9] range $0.9 < |\eta| < 2.4$. At the time of the LHC start-up, the CMS Endcap Muon system will consist of 468 six-plane CSCs. The total sensitive area of all CSC planes is about $5\,000$ m^2 with about $2\,000\,000$ wires.

The CMS cathode strip chambers are mounted on the steel disks enclosing the CMS magnet and are set perpendicular to the beam axis (Fig. 1). When viewed from inside of the LHC ring, the left and right Muon Endcaps of CMS are denoted by ME$-$ and ME$+$, respectively. There are 4 stations of chambers on each side of the detector, ME$\pm z_n$, where z_n ranges from 1 (the closest stations to the interaction point) to 4 (the outermost stations). The muon stations have 1, 2, or 3 rings of chambers, each ring being labeled as ME$\pm z_n/r_n$ (Fig. 1 (left)). The rings themselves consist of either 18 or 36 trapezoidal chambers spanning 20° or 10° in azimuth ϕ. The chambers have labels ME$\pm z_n/r_n/\phi_n$. All CSCs, except for those forming the ME$\pm 1/3$ rings, overlap to provide contiguous coverage in ϕ. A photo of the ME$+2$ disk is shown in Fig. 1 (right).

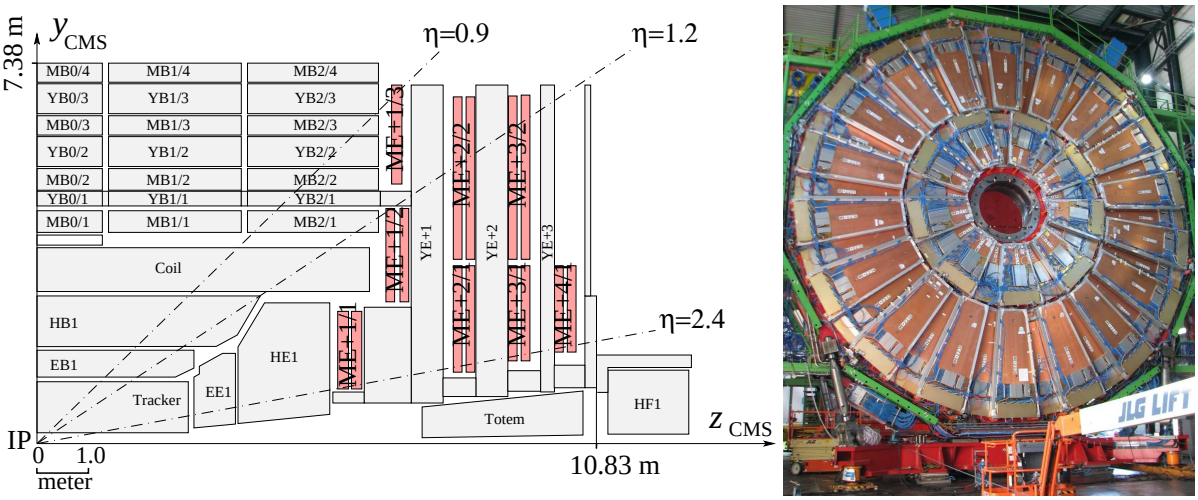

Figure 1: Left: A schematic quarter-view of the CMS detector (CSCs of the Endcap Muon system are highlighted; ME stands for Muon Endcap chambers). Right: A photo of the ME$+2$ disk and its station of cathode strip chambers.

The CMS CSCs are comprised of 6 planes of anode wires interleaved between 7 trapezoidal cathode panels (Fig. 2 (left)). Most of the CSCs have a gas gap of about 1 cm. An electron avalanche caused by a muon traversing a gas gap produces a signal on the anode wires (Fig. 2 (right top)) which induces a distributed charge on the cathode strips (Fig. 2 (right bottom)). By reading out signals from wires and strips, CMS CSCs measure 2 muon coordinates: the distance from the beam line r and the azimuthal angle ϕ in each of the 6 planes. As a muon goes through the CMS detector in the strong (4 T) magnetic field produced by the central solenoid, the change in its ϕ-coordinates allows its momentum to be measured. Hence, the requirements on the precision of measuring ϕ-coordinates are more stringent than those for r-coordinate measurements.

Wires run azimuthally and define the y coordinate of the muon track in the chamber's local coordinate system (Fig. 2 (left)). For readout purposes, the wires are ganged in groups of about 1–5 cm width. Wire group signals are amplified and shaped to a standard pulse. The general idea of a pattern of wire group hits created by a muon is illustrated in Fig. 3 (left).

Strips are milled on the cathode panels and run lengthwise at a constant $\Delta\phi_s$ width. The angular strip width $\Delta\phi_s$ varies for different chamber types from $\approx$ 2–5 mrad, while the spatial width varies from $\approx$ 4–16 mm, depending on the chamber type and local chamber y coordinate. By comparing signal amplitudes on nearby strips, the CSC electronics quickly measures the muon x coordinate to a precision of half a strip width [10]. This information, the so-called cathode comparator hits, is used by the muon Level-1 trigger. Strip signals are also digitized by 12-bit ADCs. By interpolating such digitized signals in all 6 planes, a muon's x coordinate in a chamber is measured with a precision of $\approx$ 75–150 μm. This information is available for the High-Level Trigger (HLT) and offline analyses.

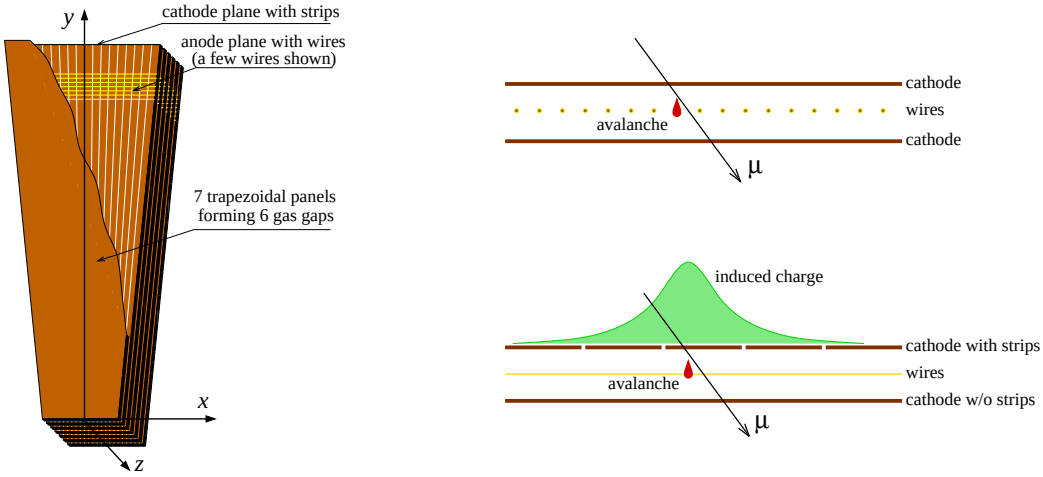

Figure 2: Left: Schematic view of a CMS cathode strip chamber. The cutout in the top panel allows one to see the radial fan-shaped cathode strips and anode wires running across the strips (only a few wires are shown). Right: An illustration of the CSC operation principle. An electron avalanche resulting from a muon traversing a gas gap produces a signal on the anode wires which induces a distributed charge on cathode strips.

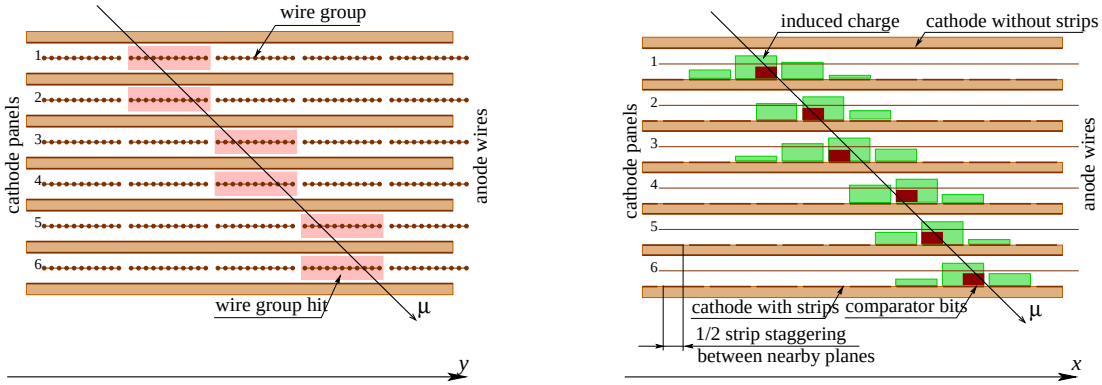

Figure 3: Left: A pattern of wire group hits created by a muon passing through a CSC. Right: A pattern of induced charges on strips and comparator half-strip hits created by a passing muon.

Figure 3 (right) illustrates a pattern of induced charges on strips and half-strip bits created by a muon.

Details on chamber locations and their internal geometrical parameters are given in Appendix A.

2 Local Charged Tracks

The CSC electronics is capable of very fast (800 ns) identification of patterns of hits in 6 chamber layers compatible with a high p_{T} muon originating from the interaction point. The fast pattern recognition is performed by Field Programmable Gate Array (FPGA) chips. The found patterns, known as Local Charged Tracks (LCT), are primitives for the Level-1 muon trigger [11]. They are also a necessary condition for reading out CSC data, i.e., CSC data are present in the Data Acquisition System (DAQ) stream for High-Level trigger or offline analyses only when LCTs have been found in that chamber.

Anode Local Charged Track patterns (ALCT) are formed from wire group hits. At every bunch crossing (25 ns), the FPGA firmware checks if anode hits in 6 planes of a chamber form patterns consistent with muon tracks originating from the interaction point. The set of wire group hits among the 6 layers from which ALCTs can be created form a bow-tie-shaped envelope (Fig. 4). Desired ALCT patterns can be programmed individually within the boundary of this envelope. We used the default patterns fully spanning the envelope, which provides the widest

acceptance. The third CSC layer is called the key-layer: for each wire group in the key-layer, the firmware seeks anode hits that lie within ALCT patterns keyed to that wire group. For a pattern to be valid, hits from at least 4 planes are required to be present in the pattern including the key-layer. Out of all ALCTs that may be present in a chamber, the electronics reports only the 2 best-quality ones per each bunch crossing, ALCT0 and ALCT1. This is adequate for the expected chamber track occupancy at the nominal LHC luminosity. The pattern quality depends on the number of planes present in a pattern and its y coordinate. The reported patterns have tags identifying the key wire groups they are associated with (marked as "$\times$" in Fig. 4).

Similarly, Cathode Local Charged Track patterns (CLCT) are searched for among comparator half-strip hits. Unlike the case of ALCTs, there are 7 CLCT patterns. These patterns are shown in Fig. 5: the straight-through pattern corresponds to high p_{T} muons, while more inclined patterns would detect softer muons. For a pattern to be valid, hits from at least 4 planes are required to be present in the pattern. In addition, 4 adjacent half-strip comparator bits are combined to form 1 di-strip bit. The electronics also checks for presence of patterns made of di-strips, which allows one to choose and trigger on highly inclined, i.e., low p_{T}, muons. The CLCT-searching firmware reports the 2 best-quality CLCTs per bunch crossing, CLCT0 and CLCT1. The pattern quality depends on the number of planes present, whether the pattern is based on half-strips or di-strips, and the inclination of the pattern. The reported patterns have tags identifying the key half-strip number with which they are associated. In the future, the number of half-strip patterns will be increased to cover the full angular range, and di-strip-based patterns will no longer be used.

Further downstream, ALCTs and CLCTs are paired to form 2-dimensional LCTs. It is these 2d-LCTs that are used as input primitives for searching for and forming full muon tracks by the Level-1 muon trigger.

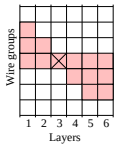

Figure 4: Wire groups bit pattern used for constructing ALCTs. The key wire group is marked with a cross.

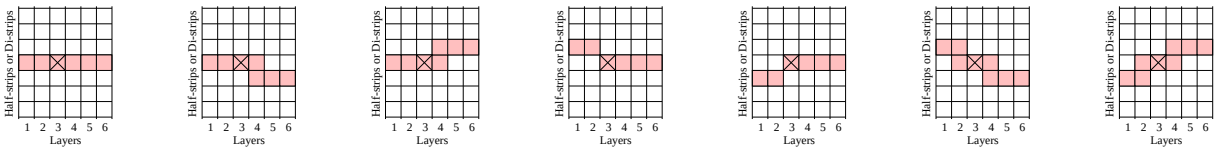

Figure 5: Comparator bit patterns used for constructing CLCTs. The key half/di-strip is marked with a cross. The straight-through pattern (left) corresponds to high p_{T} muons, while more inclined patterns would detect softer muons.

3 Magnet Test and Cosmic Challenge Setup

In the second half of 2006, during the Magnet Test and Cosmic Challenge (MTCC) [12] exercise, a substantial part of the CMS detector operated as one system. The Endcap Muon System was represented by a 60° sector of the ME$+$ endcap. Figure 6 shows the layout of chambers that were present in the MTCC in the global CMS coordinate system. A total of 36 chambers were operational during these tests. The data used in this analysis were taken with the magnetic field turned off.

To perform an unbiased measurement of the CSC efficiency for finding muon trigger primitives, we ran the CMS detector Data Acquisition with a Level-1 trigger based on the ME$+1$ and ME$+3$ chambers. The ME$+2$ chambers were not used in the trigger, but were present in the readout whenever an LCT in these chambers was found in coincidence with the Level-1 trigger. It is these ME$+2$ chambers that we used to measure the efficiency.

The overall area available for studying the LCT-finding efficiency was of the order of 23 m^2. This is an area far larger than what was available in the earlier beam tests studies [11, 13], which, by necessity, were always limited to very small chamber areas, typically of the order of or less than 10×10 cm^2.

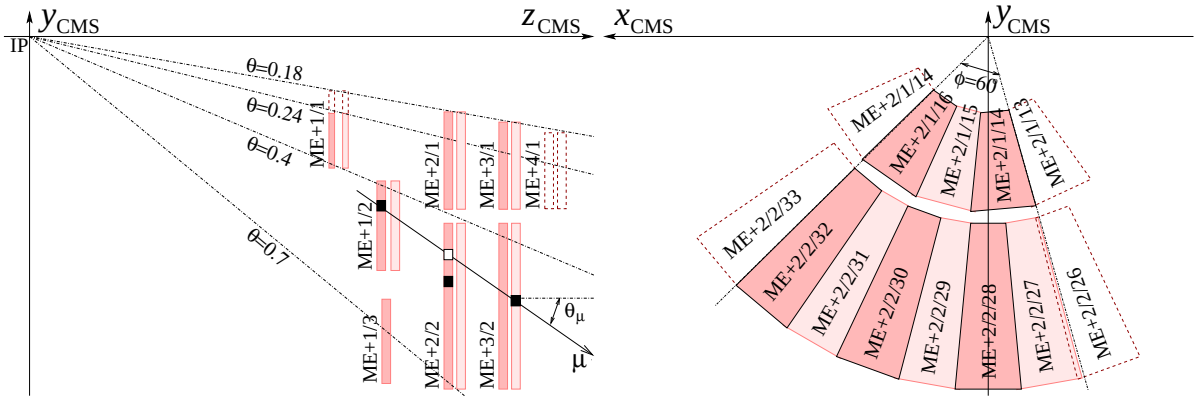

Figure 6: CSCs that took data during the MTCC. Highlighted chambers were operational during the MTCC. Left: Side view. The solid boxes schematically show the locations of ALCTs that were actually found for a muon in 3 chambers. The open box indicates the predicted ALCT position in the ME+2 station for this muon based on the measurements in ME+1 and ME+3. Right: Transverse view of the ME+2 station.

An example of typical event considered in the analysis is shown in Fig. 7. Visualization of this event was performed by the Interactive Graphics for User Analysis (IGUANA) system [14]. Wire and strip hits in 3 chambers (ME+1/2/30, ME+2/2/30, and ME+3/2/30) are represented.

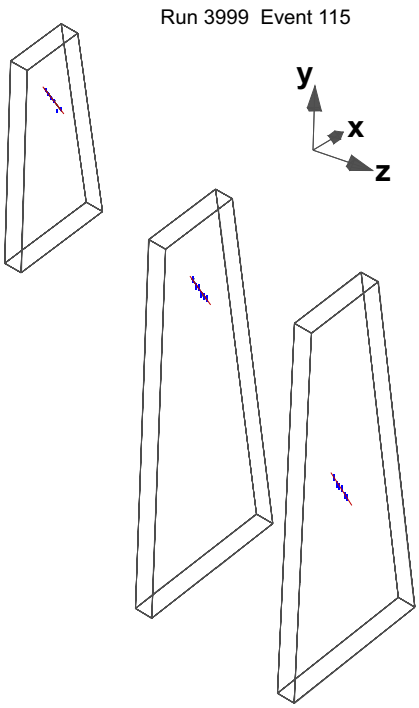

Figure 7: Screen shot of the interactive IGUANA-based event display, showing CSCs with strip and wires hits due to a cosmic muon that passed through 3 stations of the EMU system.

4 Offline Event Selection

To eliminate ambiguities in predicting the muon track position in the middle ME+2 chamber, we required one and only one Track Segment (TS) among all ME+1 chambers and one and only one track segment among all ME+3 chambers. Track segments were identified using the simple algorithm described in Appendix B. It allowed us, using information only from the ME+1 and ME+3 chambers, to predict muon track positions in the ME+2 chambers with a few millimeter precision in both the x and y directions. The prediction accuracy was mostly driven by the multiple scattering of cosmic ray muons in the EMU steel disks (see Fig. 1). Since we used runs

taken with the magnetic field turned off, the muon track was assumed to be a straight line going through the 2 space-points assigned to the ME+1 and ME+3 track segments.

The ALCT- and CLCT-finding electronics are designed to have high efficiency for muons originating from the Interaction Point (IP). We selected events where the predicted track direction would resemble "IP-like" muons. This was achieved by selecting events in which the local polar angle of the track θ_μ (see Fig. 6) predicted from track segments in the ME+1 and ME+3 stations was within 0–1 rad. In addition, the ϕ_n-number of the chambers with track segments in the ME+1 and ME+3 stations had to be the same (e.g., ME+1/3/27 and ME+3/2/27). Note that the quotes in "IP-like" are essential: we did not actually require selected muons to point back exactly to the IP; if we had, we would have had a very small event sample to work with.

Events in which the predicted tracks would miss the geometrical area of the ME+2 chambers (limited in the r-ϕ plane by upper and lower distances from the beam line as well as minimum and maximum azimuthal angles) were excluded from the analysis.

After these cuts, we ended up with 759 tracks going through ME+2/1 chambers and 14 100 tracks going through ME+2/2 chambers. There are fewer tracks through the ME+2/1 chambers because they are smaller in size and, more importantly, require more horizontal muons, which are sparse in cosmic rays. The predicted track positions in the key-layer of the ME+2/1 and ME+2/2 chambers are shown in Fig. 8.

The chamber wire planes are not contiguous from the narrow end to the wide end. There are 2 or 4 breaks of 25 mm width at approximately every 60 cm, which create 3 or 5 independent high voltage segments per plane. These break points are also used to introduce panel supports, without which the panels would bulge or cave in and stable chamber operation would not be possible. These break points, indicated by dashed lines in Fig. 8, result in dead zones. These dead zones line up horizontally and mostly effect tracks with smaller θ_μ-angle.

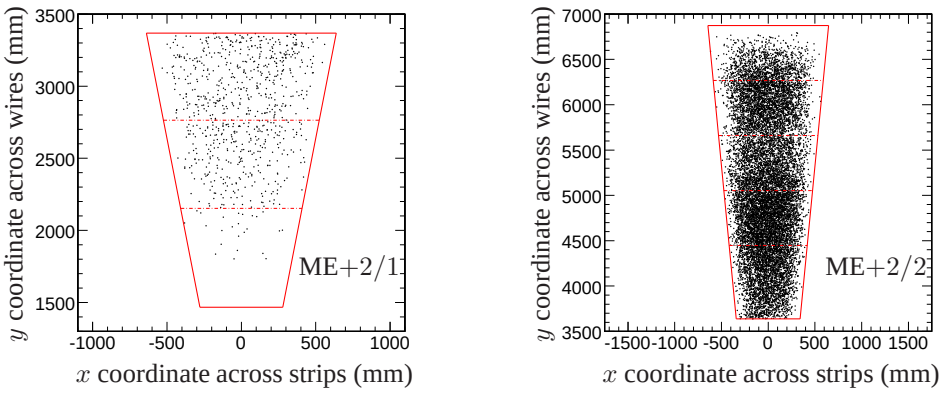

Figure 8: Predicted positions of muon hits in ME+2/1 (left) and ME+2/2 (right) chambers.

5 Efficiency Measurement

For an event to be counted as efficient, we required at least one ALCT and at least one CLCT (i.e., at least one 2d-LCT) to be reported by the ME+2 chamber through which the predicted muon should have gone.

Although we do expect some loss of efficiency near chamber edges and between high voltage segments, we first obtained the chamber LCT-finding efficiencies without any fiducial cuts. The corresponding results (the number of events with predicted tracks going through ME+2 chambers, the number of events for which a 2d-LCT was not reported by the ME+2 chambers, and the corresponding efficiencies) are given in Table 1. The average efficiency, without any fiducial cuts, was around 97%–98%.

Figure 9 shows only those predicted track positions in the ME+2/1 and ME+2/2 chambers when no 2d-LCT were reported. One can clearly see the clustering occurring around the chamber geometrical dead zones.

The efficiency depends on the local polar angle θ_μ of a muon's track as shown in Fig. 10 (left). One can see that the efficiency sags for smaller angle tracks. To lose an LCT, one needs to lose hits in 3 or more planes. A straightforward geometric analysis of how track with different θ_μ-angles cross the dead areas between high voltage segments results in the curve also shown in the figure. Although the curve is somewhat simplistic as it includes

Table 1: Efficiencies to detect muon 2d-LCTs by ME+2 chambers without fiducial cuts. The errors are statistical.

	Number of selected events	Number of events with no 2d-LCT reported	Efficiency to report 2d-LCT
ME+2/1	759	22	$97.1 \pm 0.6\%$
ME+2/2	14100	267	$98.1 \pm 0.1\%$

neither the single plane detecting inefficiency nor errors in the θ_μ-angle predictions, the data and the curve are clearly in good agreement.

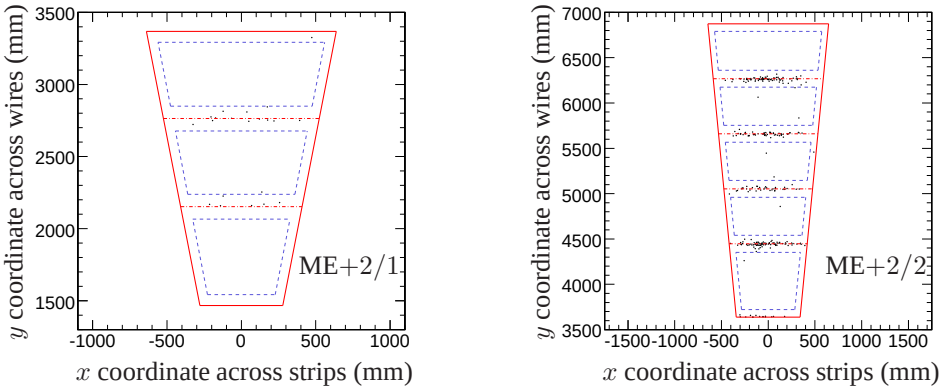

Figure 9: Predicted positions of muon hits in ME+2/1 (left) and ME+2/2 (right) chambers when LCTs in ME+2 are lost.

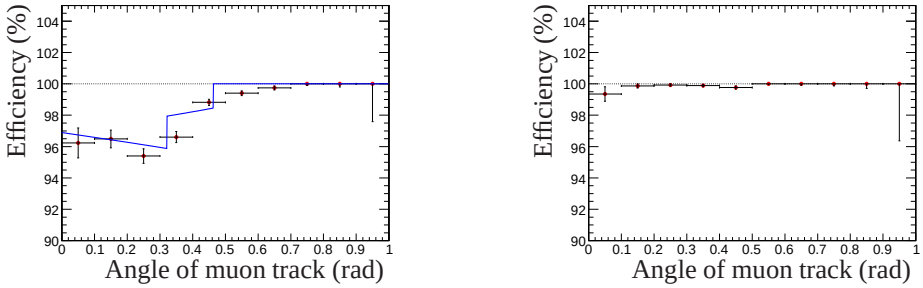

Figure 10: Efficiency to report a muon LCT as a function of track angle θ_μ without fiducial cuts (left) and after excluding "semi-dead" zones (right) in ME+2 chambers. The predicted efficiency curve based on geometric analysis is shown as the solid line.

To measure the true CSC efficiency, i.e., excluding geometrical dead zones, we applied fiducial cuts on the predicted tracks to eliminate those that would cross dead zones. The chamber areas with full acceptance are shown in Fig. 9 as dashed polygons. The borders for these areas were defined so that tracks with our selection of allowed directions would never miss 3 or more planes due to dead zones or chamber edges. These areas were reduced further by 1–1.5 cm to account for the finite precisions, σ_{dx} and σ_{dy}, with which we could predict muon track positions in the ME+2 chambers. These corrections corresponded to $3\sigma_{dx}$ and $3\sigma_{dy}$ (see Appendix B for details). After applying such fiducial acceptance cuts on the predicted tracks, only one 2d-LCTs in ME+2/1 and seven 2d-LCTs in ME+2/2 chambers were lost. In 1 of these 8 events, the 2d-LCT was actually in the neighboring chamber, 5 events had neither ALCTs nor CLCTs, and in 2 events an ALCT was reported with no matching CLCT. The CSC efficiency averaged over all chambers used in this study was found to be $99.93 \pm 0.03\%$. Details are given in Table 2. The efficiency dependence of a track angle after applying the fiducial cuts is shown in Fig. 10 (right). It is greater than 99% for all angles.

To confirm that what we measured is the efficiency to find muon-associated 2d-LCTs (rather than just noise), we

Table 2: Efficiencies to detect muon LCT in ME+2 chambers after excluding "semi-dead" zones.

	Number of triggered events	Number of events with undetected muons	Efficiency to report LCT
ME+2/1	532	1	$99.8 \pm 0.2\%$
ME+2/2	9990	7	$99.93 \pm 0.03\%$

plotted the differences between the predicted muon track x and y positions and the actual 2d-LCT0s reported by the ME+2 chambers (Fig. 11). The positions of the 2d-LCT0s in the ME+2-chambers were defined by the centers of the ALCT0 key wire groups and CLCT0 key half-strips.

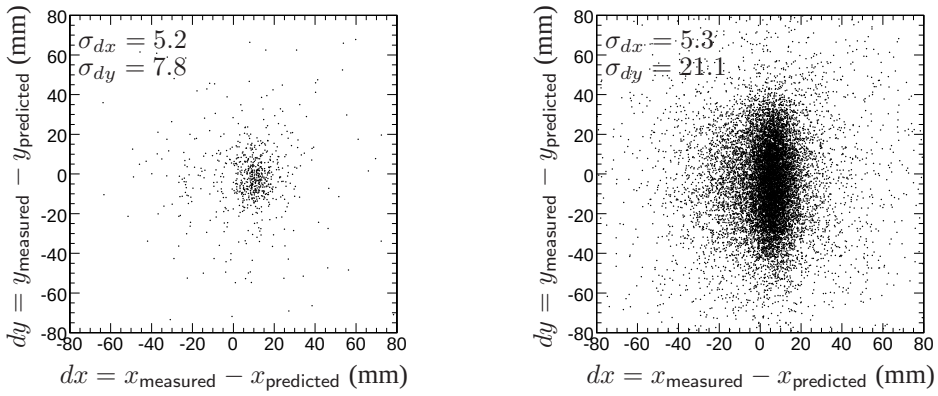

Figure 11: Muon hits residuals in ME+2/1 (left) and ME+2/2 (right) chambers.

The LCTs found in the ME+2 chambers are within ≈0.5–2 cm around the predicted positions, which is consistent with the expected multiple scattering of cosmic ray muons and the widths of the strips and wire groups. For further discussion, see Appendix B. Note that the ME+2/2 chambers are distinguished by a large $\sigma_{dy} \approx 2.1$ cm. This is because these chambers have very broad wire groups about 5 cm wide, which determines the spread of the residuals: $(5 \text{ cm})/\sqrt{12} \approx 2$ cm.

6 Conclusions

The efficiency of the CMS cathode strip chambers to report muon trigger primitives was measured with cosmic ray muons over an area of ≈23 m^2 of installed chambers. The obtained efficiency was $99.93 \pm 0.03\%$, which exceeds the design specification of 99%.

7 Acknowledgments

The authors would like to thank all our CMS colleagues and CERN staff who made the CMS MTCC exercise possible.

References

[1] CMS Collaboration, *The Muon Project Technical Design Report*, CERN/LHCC 1997-032 (1997).

[2] M.C. Fouz et al., *The CMS muon system*, Nucl. Instr. and Meth. **A446** (2000) 366.

[3] CMS Collaboration, *CMS Physics Technical Design Report Volume I: Detector Performance and Software*, CERN/LHCC 2006-001 (2006).

[4] CMS Collaboration, *CMS, the Compact Muon Solenoid: Technical Proposal*, CERN/LHCC 1994-038 (1994).

[5] The LHC study group, *The Large Hadron Collider: Conceptual Design*, CERN/AC 1995-05 (1995).

[6] D. Acosta et al.,*Large CMS cathode strip chambers: design and performance*, Nucl. Instr. and Meth. **A453** (2000) 182.

[7] Yu. Erchov et al., *Cathode strip chamber for CMS ME1/1 endcap muon station*, Phys. of Part. and Nucl. Lett. **3** (2006) 73.

[8] G. Charpak et al., *High-accuracy localization of minimum ionizing particles using the cathode-induced charge centre-of-gravity read-out*, Nucl. Inst. and Meth. **167** (1979) 455.

[9] $\eta = -\ln(\tan\theta/2)$, where θ is the polar angle.

[10] M.M. Baarmand et al., *Spatial resolution attainable with cathode strip chambers at the trigger level*, Nucl. Instr. and Meth. **A425** (1999) 92-105.

[11] CMS Collaboration, *The Trigger and Data Acquisition project, Volume I. The Level-1 Trigger, Technical Design Report*, CERN/LHCC 2000-038 (2000).

[12] CMS Collaboration, *The CMS Magnet Test and Cosmic Challenge (MTCC Phase I and II) Operational Experience and Lessons Learnt*, CMS NOTE-2007/005 (2007).

[13] D. Acosta et al., *Design features and test results of the CMS endcap muon chambers*, Nucl. Instr. and Meth. **A94** (2002) 504.

[14] G. Alverson et al., *IGUANA Architecture, Framework and Toolkit for Interactive Graphics*, ECONF **C0303241**, arxiv:cs.se/0306042 (2003).

[15] O.C. Allkofer et al., *The Absolute Cosmic ray Muon Spectrum at Sea level*, Phys. Lett. **B36** (1971) 425.

A Appendix A: CMS CSC Parameters

Parameters of chambers extensively used in this analysis are summarized in Table 3. ME$1/1b$ refers to the larger part of the ME$1/1$ chambers covering $|\eta| < 2.0$.

Table 3: Chambers parameters

Chambers	ME+						
	$1/1b$	$1/2$	$1/3$	$2/1$	$3/1$	$2/2$	$3/2$
Number of strips	64	80	64	80	80	80	80
$\Delta\phi_s$ (single strip), mrad	2.96	2.33	2.15	4.65	4.65	2.33	2.33
Strip width (narrow side), mm	4.4	6.6	11.1	6.9	7.8	8.5	8.5
Strip width (wide side), mm	7.6	10.6	14.5	15.6	15.6	15.9	15.9
Number of wire groups	48	64	32	112	96	64	64
Wire group average width, mm	31.4	26.5	49.7	16.5	17.2	48.9	48.9
z position of the wire layer closest to the IP, mm							
even chambers	5834.5	6790.1	6888.1	8098.1	9414.9	8098.1	9414.9
odd chambers	6101.5	7064.1		8346.1	9166.9	8346.1	9166.9
Distance between layers, mm	22	25.4					

B Appendix B: Track Segments Reconstructed Offline

To improve our ability to predict track coordinates in the ME$+2$ chambers based on measurements in ME$+1$ and ME$+3$ chambers, we used a very simple track segment reconstruction algorithm based on anode hits and cathode comparator bits. Using this algorithm, we could localize segments to within a few millimeters in both the x and y directions. As a result, the precision with which we could predict muon track coordinates in the ME$+2$ chambers was mostly driven by the multiple scattering of cosmic ray muons in the Endcap steel disks. Here we describe the algorithm and evaluate its performance using MTCC data.

Anode Segments (AS) were searched for among anode hits using the same pattern as shown in Fig. 4. Since muons with larger θ-angles are preferred [1)], the pattern was moved along a chamber starting from its wide side inward, one key wire group per step. If 6 layers with anode hits were present in the pattern at some step, then an anode segment was reported and all hits inside this pattern were deleted. Upon reaching the narrow end of the chamber, the procedure was repeated again with a requirement of 5 and, then, 4 layers with hits in the pattern. Anode segments were numbered sequentially, AS0, AS1, etc. The found anode segments were assigned (y_{AS}, z_{AS})-coordinates by taking the center of gravity (COG) of hits associated with them. If there was more than 1 hit per plane in a pattern, the hit weights were reduced so that the total weight per plane was always 1. In addition, a linear fit was used to evaluate the segment slope dy/dz. For a wire group width w, the expected error (RMS) on the y_{AS} coordinate would be $w/\sqrt{12}/\sqrt{6} \approx 0.12\,w$, or 2–6 mm, depending on the chamber type.

Cathode Segments (CS) were similarly searched for using half-strip comparator bits and the 9 patterns shown in Fig. 12 (they were obtained from the most recent CLCT-finding firmware). Sequentially, all 9 patterns were moved across the strips from one side of a chamber to the other. In the first pass, we looked for 6 layers with hits present in a pattern; then, for 5 layers, and, finally, for 4 layers with hits in a pattern. Cathode segments were numbered sequentially, CS0, CS1, etc. Similarly to anode segments, (ϕ_{CS}, z_{CS})-coordinates and track slopes $d\phi/dz$ were assigned to patterns. Using this technique, one would expect to achieve about 0.5–2 mm precision along the x coordinate, depending on the chamber type and muon hit location along the strips.

Anode and cathode segments were then combined to make a complete 2-dimensional Track Segment (TS). Whenever multiple ASs and/or CSs were found, we used all possible combinatorial pairings to make full 2d-TSs. If z_{CS} and z_{AS} were different, the track segment z coordinate z_{TS} was taken as $z_{TS} = 0.5 \times (z_{CS} + z_{AS})$ and (ϕ_{TS}, y_{TS})-coordinates were recalculated for the new z_{TS}-location using the $d\phi/dz$ and dy/dz slopes.

To evaluate the performance of the algorithm, we applied it to all the chambers in all 3 stations.

First, we found that the algorithm did find at least one track segment in all chambers with 2d-LCTs reported

[1)] In CMS, track segments at larger θ-angles are less likely to be due to backgrounds

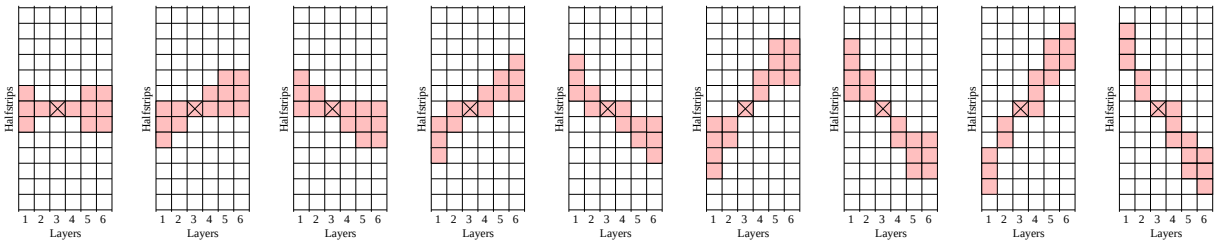

Figure 12: Comparator bit patterns used for constructing cathode segments. The key half-strip is marked with a cross.

by hardware (total of $10\,522$ events). Therefore, the efficiency of finding track segments can be estimated to be $> 99.97\%$ at the 95% CL for chambers with hardware-found LCTs. Note that chambers in which hardware did not find an LCT would not be available for further analysis (High-Level trigger or offline).

Second, using track segments found in ME$+1$ and ME$+3$ (in the same way as described in the main body of the note), we predicted track positions in the ME$+2$ chambers and compared them to the track segments found by those chambers. The residuals are shown in Fig. 13 (ME$+2/1$ chambers) and Fig. 14 (ME$+2/2$ chambers). For these plots, if there were multiple TSs reconstructed in these chambers, we used the best track segment, TS0, even if it was not the closest to the predicted track position. One can see that the dx and dy distributions for ME$+2/1$ and the dx distribution for ME$+2/2$ have core widths $\sigma \approx 3.5$ mm. The dy distribution for ME$+2/2$ has a core width $\sigma \approx 6$ mm. Also, one can clearly see that residuals are not centered around zero; this is due to the Endcap disks' misalignment during the MTCC, which was confirmed by geodesic survey.

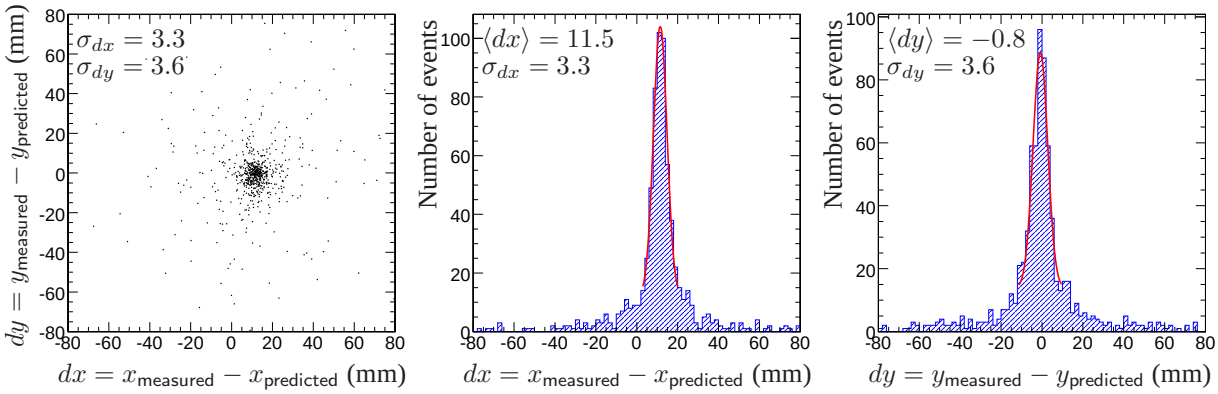

Figure 13: Muon hit residuals in ME$+2/1$ chambers after a software search for track segments and applying the "*COG*" technique to find the muon's coordinates.

To show that the obtained residuals are consistent with multiple scattering of muons, we performed the following calculations. A muon with an average inclination of 0.4 rad with respect to the horizon would lose approximately 9 GeV on its way through the whole CMS detector before hitting the Endcap Muon system (see orientation of the CSC chambers used in the MTCC, Fig. 6). A muon that hits the ME$+1/1$ chambers has to have an energy of at least 2 GeV to pass through 2 steel disks to reach the ME$+3$ station. The approximate cosmic ray muon spectrum $dN/dE_\mu \sim E_\mu^{-2.6}$ [15] is shown in Fig. 15 (left). The additional axis on this plot shows by how much the muon energy spectrum shifts after passing through CMS, just before hitting the ME$+1$ chambers. The filled area shows only the portion of the spectrum corresponding to muons that can reach the ME$+3$ chambers. Then, for a muon of a given energy, we calculated the expected, multiple scattering induced, $dN/dx(E_\mu)$-spread between the muon coordinate measured in the ME$+2/2$ chambers and the coordinate predicted from measurements in the first and third stations. After that, the 2 distributions, $dN/dx(E_\mu)$ and dN/dE_μ, were convoluted. Finally, we added the expected spatial accuracy for TS as it was estimated above. The result for ME$+2/1$ is shown in Fig. 15 (right). It is clear that the observed residuals are consistent with our simple model. The same level of agreement was observed for other chambers and projections. From these plots, we can conclude that multiple scattering is the dominant

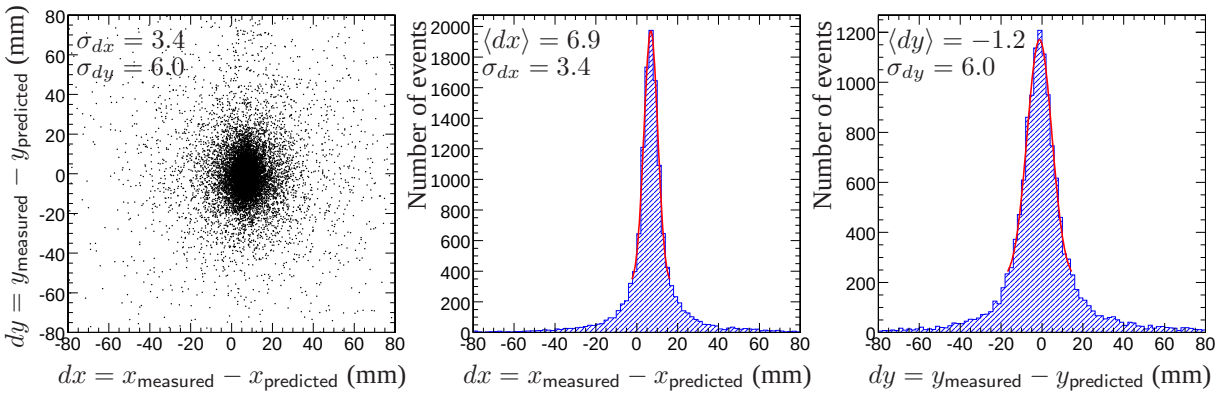

Figure 14: Muon hit residuals in ME+2/2 chambers after a software search for track segments and applying the "*COG*" technique to find the muon track segment coordinates.

contribution to the residuals of the cathode segment measurements. The anode segment measurement precision in ME+2/1 chambers is also dominated by multiple scattering. The large ME+2/2 chambers have wide wire groups, which limits the accuracy of coordinate measurements to 6 mm.

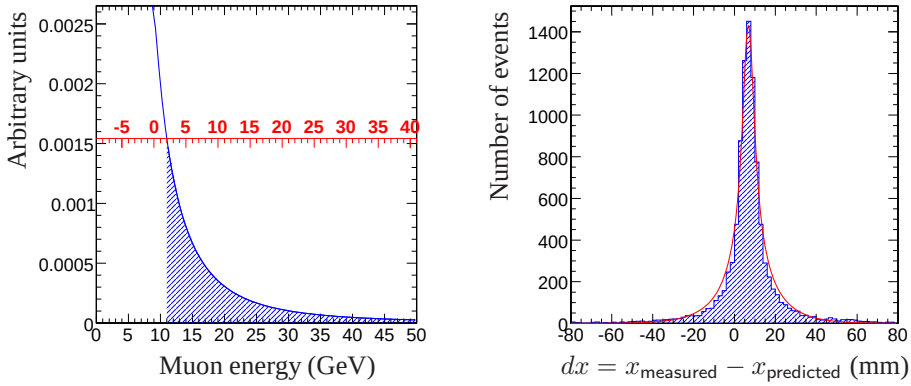

Figure 15: Cosmic ray muon spectrum (left). Muon hit dx-residuals in ME+2/2 chambers (right).

Next, we looked at the number and quality of the found segments (the algorithm allows us to find as many segments as there are in a chamber). Distributions of the numbers of found anode, cathode, and combined 2-dimensional track segments (AS, CS, and TS) in ME+2 chambers are shown in Fig. 16.

Table 4: Number of events (with fraction in brackets) for different numbers of anode (AS) and cathode (CS) segments in the ME+2 chambers.

ME+2		AS		
		1	2	3 or more
CS	1	10000 (95.1%)	113 (1.1%)	6 (0.06%)
	2	160 (1.5%)	171 (1.6%)	13 (0.12%)
	3 or more	5 (0.05%)	17 (0.16%)	26 (0.25%)

Table 4 shows the numbers of events with different combinations of found segments. About 95% of the events were simple as they had only 1 AS and 1 CS (and, therefore, only 1 2d-TS). All events with multiple segments were visually scanned using an event display. Most of the events with 1 anode segment and 2 cathode segments (and *vise versa*) looked like they had 2 close-by tracks and the anode (or cathode) segment searching algorithm was not able to separate them. Events with 2 anode segments and 2 cathode segments were either clean 2-track events or more complex broad showers. The final ≈1% of events with 3 or more segments in 1 or both projections

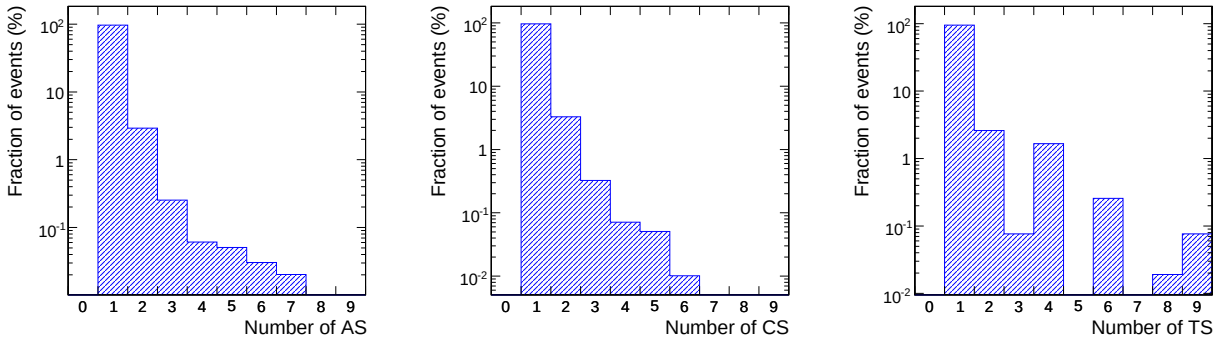

Figure 16: Distributions of numbers of anode (left), cathode (center), and combined 2-dimensional track segments found in the ME+2 chambers.

were all due to broad showers with many hits spread over the chamber. It is worthwhile pointing out that, in cases when there were 2 or more track segments found in the ME+2 chambers, the reconstructed segment closest to the predicted muon track position typically ($> 80\%$) had a better quality than all other segments. Fig. 17 shows the distribution of the pattern qualities for the closest and all other segments.

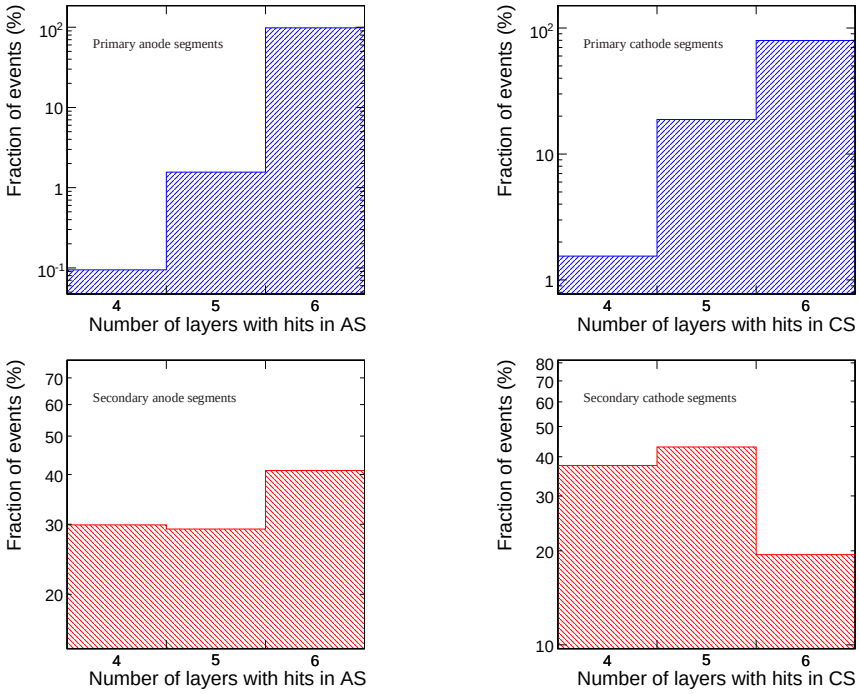

Figure 17: Quality (number of layers with hits) distributions of primary (left plots) and secondary (right plots) segments in ME+2 chambers. The primary segment is the one closest to the predicted muon track position; all others are secondary.

Finally, we benchmarked the CPU performance of the algorithm using MTCC data. The average time required to reconstruct all segments in a chamber with at least 1 track was approximately 0.3 ms (Intel Pentium M 1.6 GHz processor). At this speed, the algorithm is well suited for the High-Level trigger.